Renewable and Sustainable Energy Reviews 34 (2014) 98–109

Contents lists available at ScienceDirect

Renewable and Sustainable Energy Reviews

journal homepage: www.elsevier.com/locate/rser

Energy of marine currents in the Strait of Gibraltar and its potential as a renewable energy resource

María Concepción Calero Quesada*, Jesús García Lafuente, José Carlos Sánchez Garrido, Simone Sammartino, Javier Delgado

Physical Oceanography Group, University of Málaga, Spain

ARTICLE INFO

Article history:
Received 18 October 2013
Received in revised form
11 February 2014
Accepted 18 February 2014
Available online 21 March 2014

Keywords:
Strait of Gibraltar
Energy fluxes
Tidal energy
Unidirectional currents

ABSTRACT

A non-hydrostatic hydrodynamic model of the Strait of Gibraltar with high spatial and temporal resolution has been used to assess suitable areas for energy extraction from marine currents. The model shows great spatial variability of the available energy flux, ranging from 200 W m^{-2} to more than 1800 W m^{-2}. In addition to the mean energy flux, other properties and characteristics of the flow such as permanence and direction of the currents, vertical shear or occurrence of unwanted high frequency internal waves have been merged into an index that is used in this work as a proxy for the suitability of a given place to install a power plant. This index highlights two zones gathering the required conditions: the subsurface layer of the eastern half of the strait and the near-bottom layer of Espartel sill at the westernmost gateway of the strait.

Contents

* Correspondence to: Campus Teatinos s/n, 29071 Málaga, Spain. Tel.: +34 952 132 849.

http://dx.doi.org/10.1016/j.rser.2014.02.038
1364-0321/

1. Introduction

Renewable marine energy can be obtained from wind waves and swell, tides, ocean currents and from ocean salinity and temperature gradients. Many different devices are employed at this aim, such as the direct-drive converters that transform the wave mechanical energy in electrical power, the hydrokinetic turbines that convert the kinetic energy of the moving mass of water into electricity in the case of marine currents, or the thermal oceanic plant, producing energy by the thermic differences between deep and surface waters [1]. Ocean contains a large amount of unexploited clean renewable energy resources that can play a significant role in the future of worldwide energy portfolios. This kind of energy will supply future electrical energy needs in the world: the U.S. Electric Power Research Institute (EPRI) and the National Renewable Energy Laboratory (NREL) estimate that the total potential of all the combined ocean renewable energies in United States currently exceeds the national electric energy needs. A total of 13 GW of new hydrokinetic technologies could be deployed by 2025, supplying at least the 10% of the USA electrical needs [2]. Wave and tidal current energy could potentially supply the 15% of the UK's electricity needs [3] and wave energy is likely to have a significant role in Australia electric policy with the highest capacity expected (449 GW from 2023 to 2032) [4].

Several technologies and devices are currently operating with different efficiency depending on the available energy and the device performance and maintenance [1]. The exploitation of renewable energy from ocean waves is widely developed in several countries as Australia, Americas, Portugal, South Africa, parts of Scandinavia, United Kingdom [3], and Ireland [5]. Wind waves energy extraction has different technologies [6] and modes of operation [7] with high energy potential (of the order of TW/yr). Some of the most interesting ongoing projects are the Pelamis Wave Power (PWP) in Portugal (2.25 MW), in Orkney (3 MW) and Cronwall (5 MW) in UK [8].

1.1. Tidal energy resource

Marine currents carry a huge deal of energy, too, but this technology is currently under pilot phase or research projects [9]. Some of the most suitable places to extract this type of energy are Ireland, the Amazon River, the English Channel, the Strait of Gibraltar [10], Fiji Island [11], the Strait of Messina [12], the southern coast of Iran [13] or South Korea [14]. Most of the plants are already functioning, as the case of the coast of Welsh (UK) with its 8 MW, while others are currently being completed, as the one in Korea that will supply 300 MW by 2015 [8]. In some places the extraction of marine energy can be combined by two types of energy, as the case of wave and tidal mixed systems in UK [15].

There are different energy conversion systems in MCTs: rotating devices and reciprocating devices. The extraction of energy from ocean currents by rotating devices has the same physical basis as the extraction from wind and a similar technology. These are named marine current turbines (MCTs). The generated power is directly proportional to the fluid density and the cube of the speed. In places suitable for the extraction of marine energy, ocean currents are typically one order magnitude less than wind speed, but the sea water density is about three orders of magnitude greater than the air density and, therefore, the power generated is of the same order of magnitude in both environments.

MCTs can have two different configurations: the axial turbines, the most frequently employed, where the axis rotates horizontally parallel to the current stream and, with a special configuration of the blades (variable pitch) can operate in opposite flows, and the cross-flow turbines where the main axis is vertical and the blades are perpendicular to the main stream, being able to operate with flow from any direction [4,9].

An intense work of design and optimization is currently being developed in this field. While all hydrokinetic devices operate on the same conversions principles regardless of their areas of applications, a set of subtle differences may appear in terms of design and operational features of the farms. These include: design of the turbine (size, directionality and placement), operation (flow characteristics, water density, control resource and prediction) and end-use (grid-connectivity) [16]. Many studies indicate different types of turbines, for instance, the Evopod tested in Ireland or the Gorlov in USA, or the most promising, Delta Stream Turbine or the Neptune Tidal Stream Device (2.4 MW of capacity) [10].

Several test models claim a superior performance of MCTs located in marine channels than others installed in open flows, the latter being more similar to windmills, resulting in an increase of both average and peak power coefficient [17]. In general MCTs present more technical limitations than wind turbines: the closer proximity of the sea surface and the seafloor [18], the damages on the turbine blades caused by cavitation [18] and other effects related to the higher density of sea water with respect to the air. In many cases it results in the failure of the device, such as the blade fracture on the Open-Hydro 16-m installed in the Bay of Fundy or the Atlantis AR1000 [19]. Once the rotor is in motion, the blade section starts to experience a relative component of tidal current velocity at various angles of attack depending of the blade parameters [20]. For all these reasons, the presence of a strong current and the persistence of a flow in a site are not sufficient conditions to ensure its suitability for the installation of a turbine farm [21].

Besides the optimal design of the MCTs or their components, the hydrodynamic interactions between turbines may have significant impact in the efficiency of the devices and the electrical power output decays considerably. The two most important control variables for energy cost are the farm size and the turbine distribution in a farm [22]. Different models are used to find the optimal configuration of tidal turbine farms, by the solution of an optimization problem [23]. On the other hand, there are different types of devices that operate in specific conditions and prototypes still under development, whose technical characteristics can be adapted to ocean currents. For instance, the Northeast Normal University in China, developed a floating horizontal axis turbine provided with a flex shaft with a vertically arranged generator designed to avoid some disadvantages of horizontal axis turbine, such as needing pitch adjusting and efficiency dropping in reverse flow [24]. In Ria de Arousa, Spain, a parametric approach based on four performance parameters was proposed to compare two types of turbines, the Evopod and the Gorlov. It was found that the Evopod achieves greater site-specific turbine efficiency and energy output whereas the Gorlov turbine presents higher availability and capacity factors or, in other words, more operation hours and equivalent hours per year, essentially due to its lower cut-in velocity and power rating [25].

1.2. Marine currents in the Strait of Gibraltar

The Strait of Gibraltar holds areas where ocean currents are strong, around a velocity of 2 m s^{-1} [26,27] compared with 3 m s^{-1} in the Strait of Messina [12] or about 2 m s^{-1} in Ireland [28], which makes it suitable to install power marine farms. The strait is the scenario of a two-way exchange of marked spatial variability induced by interaction of the flow with the several topographic constraints as Tarifa Narrows (TN hereinafter), Camarinal Sill (CS) and Espartel Sill (ES) shown in Fig. 1 [29–32]. Atlantic water, less saline and warmer, flows at the surface into the Mediterranean while a Mediterranean undercurrent, saltier and

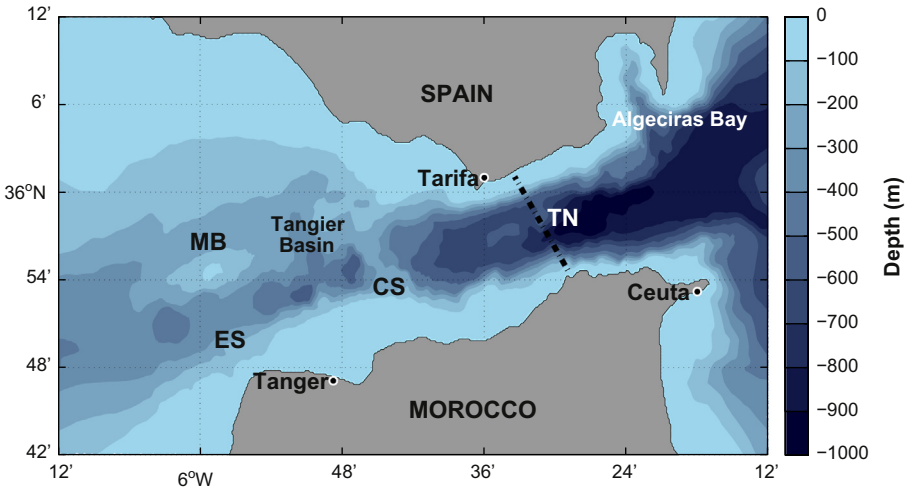

Fig. 1. Bathymetry of the Strait of Gibraltar showing the toponyms mentioned in this study: ES stand for Espartel Sill, CS for Camarinal Sill and TN for Tarifa Narrows, the narrowest section of the strait. The asterisk over Espartel sill indicates the location of a long-term monitoring station mentioned in the text.

cooler, flows out into the Atlantic. Numerical [27,33–35], theoretical [31,36,37] and experimental [27,29,38] models/analysis suggest that TN exerts hydraulic control on the inflow while CS and ES do so on the outflow, offering a scenario of hydraulically controlled exchange. Therefore, the flows in the strait occur mainly along its axis in two principal orientations: 10–15° from the east counterclockwise and 190–195°, the opposite orientation.

This two-way exchange is strongly modulated by tides that are intense enough to reverse the instantaneous flow in most areas and depths of the strait twice a day and flood the hydraulic control at CS [27,29,34,38]. Hydraulic controls at TN and ES are much less influenced by tidal flows and are quasi-permanent features [34,38,39]. Therefore, the surface Atlantic stream nearby and east of TN keeps flowing eastwards permanently while the deep Mediterranean water does the same to the opposite direction nearby and west of ES, featuring two zones of unidirectional flow regardless of tidal forcing [27,29,32,38].

A remarkable feature linked to tides is the formation of a large amplitude internal hydraulic jump over the western edge of CS during the rising tide due to the supercritical-to-subcritical transition of the Mediterranean undercurrent downstream the sill [30,40,41]. The jump is released when the Mediterranean current weakens (about 2 h before high water) and the hydraulic control at CS is lost. It progresses to the Mediterranean as a tidal bore, generating a train of large amplitude, short-period internal waves along its leading edge [35,38,42] whose associated wave-velocity field induces remarkable fluctuations able to change the total velocity by more than 1 m s^{-1} in few minutes. These fluctuations may be usable or not for extracting energy, depending on the characteristics of the devices [43,44] but, in general, of such large amplitude and high frequency oscillations are unwanted for technical reasons and will be considered as noise in the present study [45]. Notice, however, that these waves do not fulfill the most important noise characteristic, which is its random nature. Actually they are predictable [30,35,41,42] because their appearance is strictly linked to tides, an archetypical periodic phenomenon.

Atmospheric forcing also induces moderate fluctuations of the flow speed in the subinertial frequency band (few days to weeks) [46,47]. The estimation of energy fluxes and their variability in the Strait of Gibraltar should take into account this forcing. However, the subinertial fluctuations occur at relatively low frequency for which the response of the exchange can be considered as a succession of steady-states (quasi-steady fluctuations [36]). It means that the final solution can be achieved as the linear superposition of the flows exchanged in absence of atmospheric forcing and the barotropic flow induced by that forcing. The situation is completely different in the case of tides because the strength and frequency of tidal flows produce about strong nonlinear interactions between mean and tidal flows that invalidate any linear superposition. For this reason, this work focuses on the energy fluxes in the strait that is only forced by tides, and addresses the effect of meteorologically induced subinertial fluctuations on these fluxes briefly in Section 5.

The paper is organized as follows. Section 2 describes the high resolution numerical model that has been used, which has been employed in previous studies and has shown to reproduce satisfactorily the hydrodynamics of the exchange at tidal frequencies [35]. Section 3 computes the energy fluxes averaged over different periods and vertical layers in order to assess the suitability of the different areas of the strait and identify other hydrodynamic parameters of practical relevance for technological issues. In Section 4 all the previous information is merged into a single quality function that helps identify the most suitable places to install marine-current power plants. The subinertial modulation of the flow is briefly addressed in Section 5 and conclusions are shown in Section 6.

2. Methodology

In order to obtain a synoptic estimation of the flow in the area of study, aimed at calculating the energy fluxes there, a numerical approach has been applied.

2.1. Numerical model

The numerical model is the Massachusetts Institute of Technology general circulation model (MITgcm), which solves the fully non-linear non-hydrostatic Navier–Stokes equations under the Boussinesq approximation for an incompressible fluid. Next we briefly outline the model setup and its initialization for the numerical simulation used in this study. Further details on the model configuration, validation and performance can be consulted in [48].

The model formulation includes implicit free surface and partial step topography [49,50] and its domain extends from 6.3°W to 4.78°W that is discretized by non-uniform curvilinear orthogonal horizontal grid of 1440×210 points. The along-strait spatial resolution, Δx, is between 46 and 63 m in CS area and is

always less than 70 m between ES and TN. The across-strait spatial resolution, Δy, is less than 340 m in the middle of the strait between ES and CS, 175–200 m in CS and less than 200 m between CS and TN. The model has 53 vertical levels 7.5 m thick in the upper 300 m that increases gradually until 105 m maximum thickness for the remaining 13 deeper levels.

The initial conditions of temperature and salinity were derived from the climatologic Medar–MedAtlas Database [51] for the month of April. The steady two-way exchange is obtained by laterally forcing the model with the mean velocity, temperature, and salinity fields extracted from the outputs of the model developed by Sannino et al. [33], which aimed at the study of the mean water exchange through the Strait of Gibraltar and its internal hydraulics. Wave reflections at the open boundaries were minimized adopting the flow relaxation scheme proposed by Carter [52] for the velocity field. A spin-up period of 11 days of simulation was necessary to achieve the steady state without tidal forcing. Subsequently, tidal forcing was introduced by imposing the barotropic tidal current of the main diurnal (O_1, K_1) and semidiurnal (M_2, S_2) constituents at the open boundaries and leaving the model to reach a periodic stationary solutions, which was achieved after 8 days approximately. Then the model was run during a climatological month to generate outputs of the different baroclinic fields every 20 min, which is the dataset analyzed in this study.

A similar approach has been employed by the Georgia Tech Research Corporation who utilized a ROM system to obtain the intensity of tidal currents in the United States [53,54].

2.2. Energy flux computation

The along-strait component of the energy flux has been computed according to

$$E = \frac{1}{2}\rho(u^2+v^2)u \tag{1}$$

where u is the along-strait component of the velocity, v the cross-strait component and ρ the density of sea water that, for the purposes of this study, has been taken as constant ($\rho = 1027.5\ \mathrm{kg\ m^{-3}}$). The across-strait component could be calculated similarly but the prevalence of along-strait over cross-strait velocity makes that component negligible. Only the along-strait energy flux is considered in the subsequent calculations.

The energy flux has been calculated at each point of the 3D grid. These values have been vertically averaged in the layers defined in Table 1. The upper part of the water column, (0–26.25) m, has been excluded since it is not exploitable for maritime safety reasons. Although the Strait of Gibraltar holds areas deeper than the last layer in the table (Fig. 1), they are not of practical interest because of the great depth and the weakness of the currents. The contoured energy flux at k-th vertical layer has been then computed as

$$E_k(x,y) = \frac{1}{N_k}\frac{1}{N_t}\sum_{i=1}^{N_t}\sum_{j=1}^{N_k} E(x,y,z_j,t_i) \tag{2}$$

where N_t is the number data within the selected time intervals and N_k is the number of grid points within vertical layer k. Obviously the estimated energy flux depends on the interval over which the time average is carried out.

Table 1
Layers and their range depth used for the vertical average of the energy flux. Last column indicates the number of grid points inside each layer.

Layer	*Range depth* (m)	*Grid points*
1	26.25–71.25	7
2	71.25–116.25	7
3	116.25–161.25	7
4	161.25–206.25	7
5	206.25–273.75	10
6	273.75–326.25	6
7	326.25–532.50	6

3. Flow characteristics

With regards to the suitability of a marine region for renewable energy, the most important variable is the available energy flux in the zone although there are also other characteristics of the flow that are relevant. All of them are addressed in the next subsections.

3.1. Averaged energy fluxes

Fig. 2 shows the temporal mean value of the energy flux in the selected layers (actually, the mean value of the climatic April used in the simulation). The mean has been computed using absolute values (the energy flux in Eq. (1) is positive (negative) if the flow moves to the east (west)) in order to determine an upper bound to the available energy flux.

Layer 1 (Fig. 2a) presents moderate values over the central area of the strait associated with the Atlantic inflow and larger fluxes over CS. Layers 5 and 6 show the highest fluxes in the western part of the strait, in the Mediterranean outflow (Fig. 2e and f). Values in the intermediate layers 2–4 are low except in a narrow band over CS (Fig. 2b–d) because they embrace partially the interfacial layer where the velocity is small. Layer 7 (Fig. 2g) also shows very reduced values in the eastern half of the strait, where the Mediterranean outflow moves to the west slowly, and high values west of ES where the outflow plunges down in the Atlantic Ocean as a density current. This short overview indicates that layers 1, 5 and 6 deserve further analysis while the remaining layers are of secondary relevance and are no longer considered. Layer 5 shows spatial patterns very similar to layer 6, a reason for which – and for the sake of conciseness – we hardly present maps for that layer.

3.2. Other relevant parameters (indicators)

The preliminary analysis carried out in the previous section hides the high spatial-temporal variability of the flows and, hence, energy fluxes in the strait. See, for instance, the fortnightly variation of the energy flux in layer 1 from spring (Fig. 3a) to neap (Fig. 3b) tides. Fig. 3c and d shows that the energy flux in this layer is mainly achieved by positive (towards the Mediterranean Sea) flows while it diminishes if only periods of negative, westward flows are considered in the time average.

A fundamental aspect in the installation of turbine farms is the selection of the technology employed, namely, the MCTs. For these reasons and regarding the performance of the devices, it is certainly worth analyzing other time-varying parameters of the flow, rather than only the energy flux as done in [53,54]. Five of such time-varying parameters are considered in this study. The time interval over which we have calculated their values is the whole month of the model.

3.2.1. Time interval during which the energy flux is above a threshold value (TAT)

Many kinds of MCTs have a threshold speed below which they are not energetically efficient and it is therefore reasonable to define a parameter that accounts for this limitation. Time interval

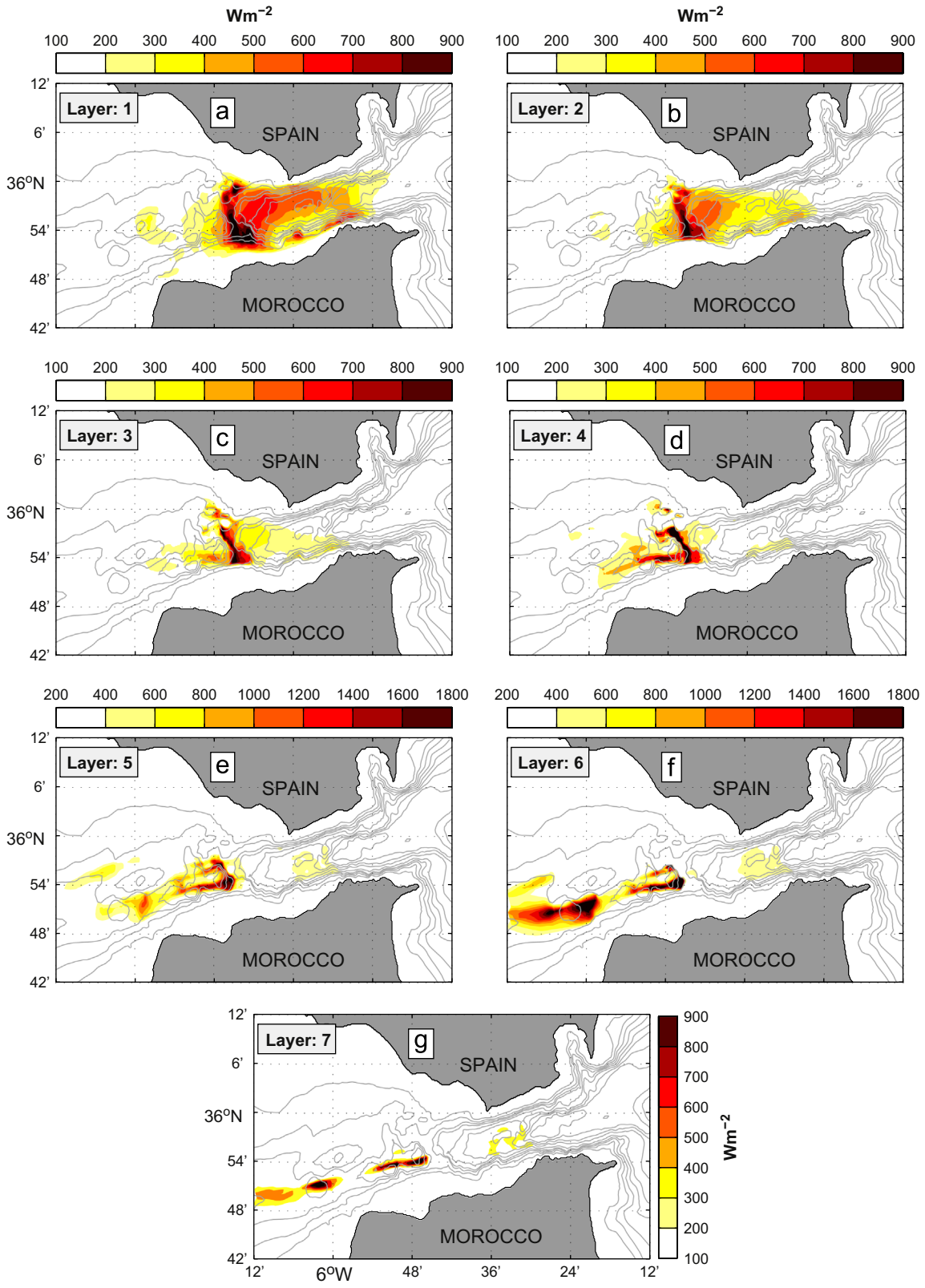

Fig. 2. Mean energy flux in the layers indicated in Table 1 and shown in the insets. The color bar, common for all panels, indicates the energy flux in W m^{-2}.

during which the energy flux is above a threshold value (TAT) is expressed as the percentage of time that the energy flux holds above the selected threshold, which in this study has been set to 200 W m^{-2} corresponding to a flow speed of 0.73 m s^{-1} according to Eq. (1). Fig. 4 presents the spatial distributions of TAT in layers 1 and 6, which are the only ones that show values above 50% over an extended area. Layers 2–4 (not shown) have patterns similar to layer 1, with smaller percentages over a smaller area (basically CS), while layer 5 (not shown) recalls layer 6 with significantly lower percentages. Regarding this indicator, the zone of ES exhibits the

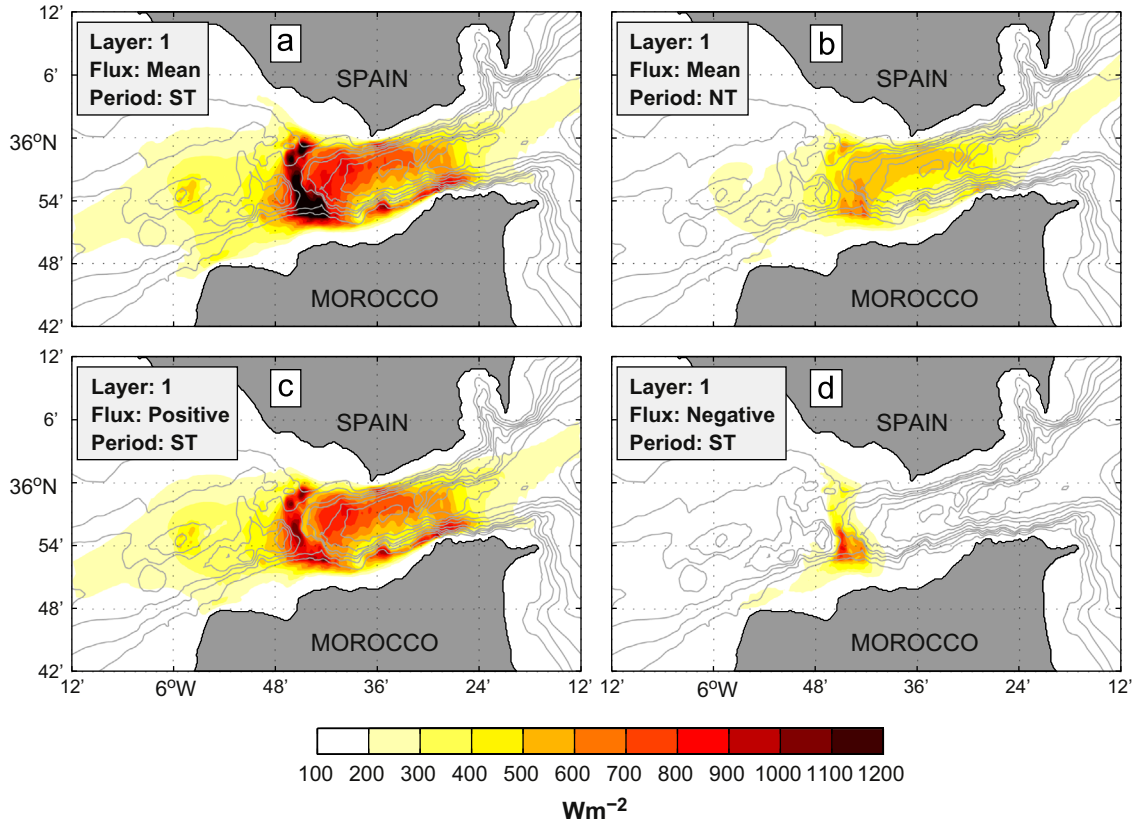

Fig. 3. Panels (a) and (b): Mean energy flux in layer 1 during spring (ST) and neap tides (NT), respectively. Panels (c) and (d): Mean energy flux associated with positive (eastward) and negative (westward) flow during ST period.

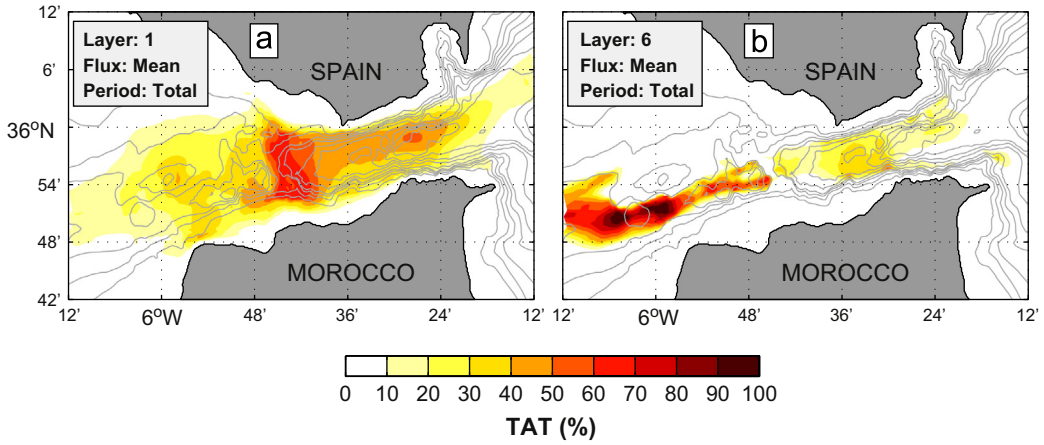

Fig. 4. Percentage of time when the mean energy flux (TAT parameter in the text) is greater than 200 W m^{-2}. Panel (a) is for layer 1 and panel (b) is for layer 6.

best conditions, with percentages over 90% in area of approximately 60 km^2.

3.2.2. *Time interval during which the energy flux does not change sign (TFP)*

Some devices only extract energy from marine currents when they are oriented upstream, that is, when they are pointing to the direction the current comes from [9]. The time interval during which the energy flux does not change sign (TFP) is of interest for such devices whenever they are mounted on structures that keep them facing at a fixed, pre-selected direction. TFP is also expressed as a percentage.

Fig. 5a presents the TFP of positive sign in layer 1, that is, the percentage of time the current in this layer flows towards the Mediterranean. As expected here, TFP is higher than 50% everywhere in the strait area (any value below 50% would indicate a prevalence of westward flow) with enhanced values in the eastern half of the strait due to the internal hydraulics of the exchange. The opposite is observed in the deep layer 6 (Fig. 5b) where TFP is nearly 90% for negative flow (towards the Atlantic) in the west half of the strait and, particularly, over ES area, remaining above 50% elsewhere.

3.2.3. *Time interval during which the flow lays along a given direction (TFU)*

Even when the energy flux does not change sign, the direction of the flow can fluctuate, decreasing the efficiency and performance of

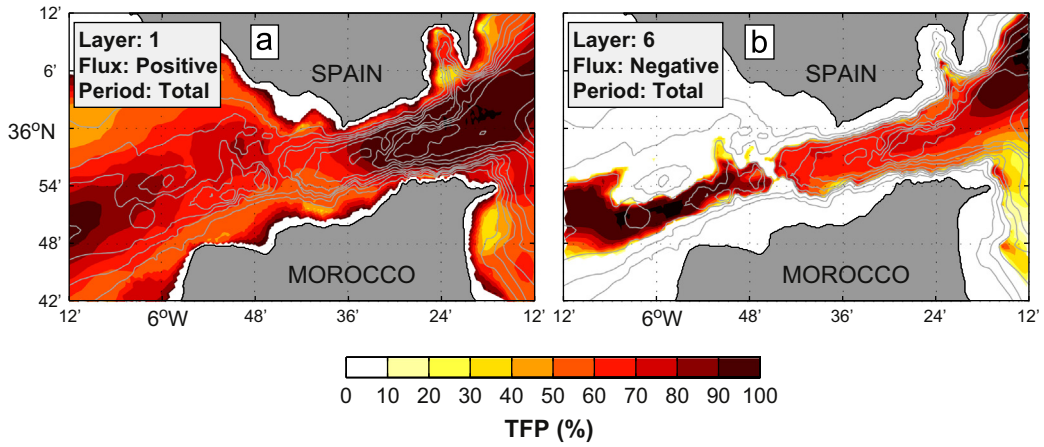

Fig. 5. Percentage of time during which the energy flux does not change sign (TFP parameter in the text). Panel (a) corresponds to positive (eastward) energy flux in layer 1. Panel (b) is negative (westward) energy flux in layer 6.

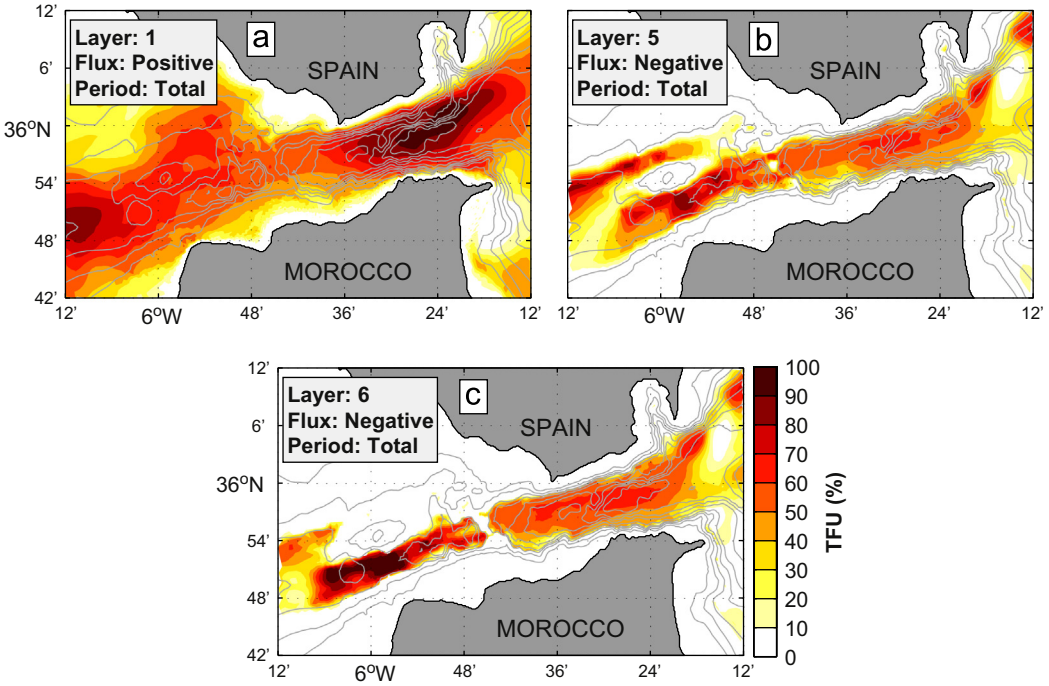

Fig. 6. Percentage of time during which the energy flux keeps the direction within given intervals (TFU parameter in the text). Panel (a) is the case of energy flux toward the Mediterranean Sea within $[-25^{\circ}, 25^{\circ}]$ in layer 1. Panel (b) is the same for layer 6 within the interval $[160^{\circ}, 210^{\circ}]$ (towards the Atlantic Ocean).

the device [22]. A suitable condition is that the flow keeps tight along a favored direction, which obviously would be the axis of the strait in this case. Again, time interval during which the flow lays along a given direction (TFU) is expressed as a percentage. Two directions have been considered with an angular tolerance of 25°: the first one towards the Mediterranean along the axis, whose limits have been set to $[-25^{\circ}, 25^{\circ}]$ and the second one towards the Atlantic within the interval $[160^{\circ}, 210^{\circ}]$. Although this parameter overlaps with TFP, it is more restrictive and identifies areas of rather unidirectional flows, a very crucial condition for the aforementioned devices [9,20].

Fig. 6a, which shows TFU in layer 1, indicates that in the central channel the average energy flux is mainly towards the Mediterranean, the percentage increasing to almost 90% to the East of TN. Recalling the results shown in Fig. 5a it is clear that the positive energy flux in this area is very directional, with only small fluctuations around the direction of the axis of the strait. Over CS, the TFU percentage is around 50%, significantly less than the ~70% of TFP there visible in Fig. 5a. Instead, the direction of the flow over CS has greater fluctuations than in the eastern strait, which makes CS a less suitable area regarding this parameter. Fig. 6b and c presents TFU in layers 5 and 6, respectively. As expected, the general pattern is the opposite to layer 1 with negative flows most of the time, particularly in the central channel. The percentage in layer 6 reaches nearly 100% in ES area and it is slightly less in layer 5. Over CS, TFU is around 50% (Fig. 6b), which indicates important fluctuations of the flow direction, much like the case of layer 1 already discussed. In summary, the eastern part of the strait in layer 1 and the western part in lower layer 6 are the best areas regarding TFU, a non-surprising result that stems from the hydraulic control associated with the internal hydraulics of the strait [34,38,39].

3.2.4. *High frequency phenomena or noise (FN)*

As mentioned in Section 1, the high frequency internal waves periodically generated in the strait may contribute negatively to the mean lifetime of some devices due to the rapid fluctuations of

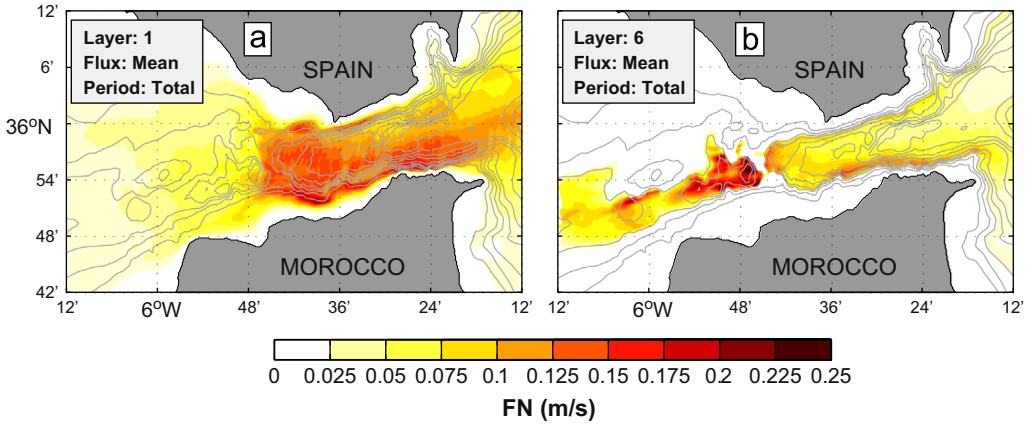

Fig. 7. Noise or RMS high frequency velocity (FN parameter in the text). Panel (a) is for layer 1 and panel (b) is for layer 6.

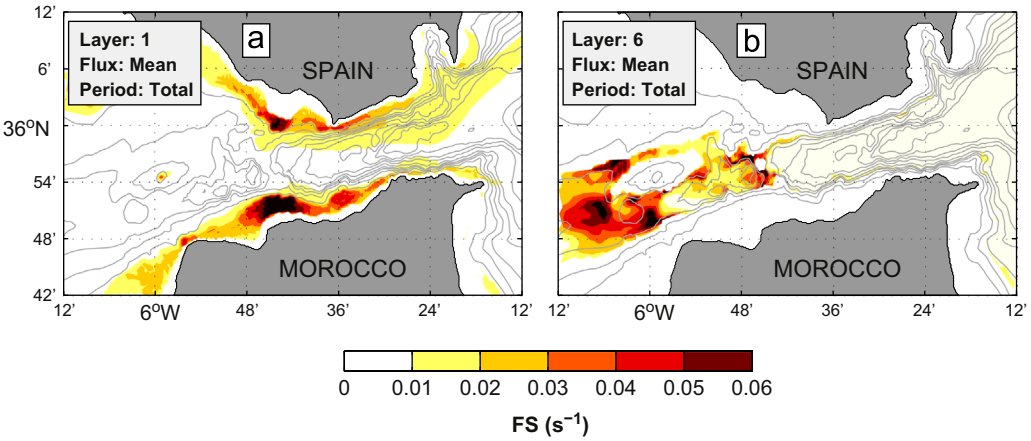

Fig. 8. Velocity shear (FS parameter in the text). Panel (a) is for layer 1 and panel (b) is for layer 6.

the velocity field. For this reason they can be considered as noise, which has been quantified as the root mean square of the high-pass velocity series obtained after filtering the original series with a numerical filter of 2 h^{-1} cut-off frequency. This indicator, high frequency phenomena (FN), has therefore units of m s^{-1}.

Fig. 7a and b shows FN in layers 1 and 6, respectively. It is well-known that internal waves are mainly found in the eastern half of the strait progressing to the Mediterranean from CS, where they are generated. Fig. 7a clearly reflects this fact and shows that FN in the upper layer 1 concentrates at east of CS. Similar patterns are found in layers 2 and 3 (not shown) with FN decreasing toward the seafloor in this area. From layers 4 to 6, the spatial pattern changes and FN starts showing significant values west of CS due to supercritical-to-subcritical flow transitions that takes place in the Tangier Basin [35,38,42]. Fig. 7b illustrates this feature and also (and more importantly) that FN is reduced drastically over ES to increase again westwards of this sill due to new hydraulic transitions [35].

3.2.5. Vertical shear of the flow (FS)

Blades of a wind-like turbine, working undersea, are subjected to forces typically 10 times stronger than the ones undergone in air. The mean lifetime of the turbine, especially of those with horizontal axis depends on vibrations supported by the rotor axis, which are enhanced in sheared flow. Vertical shear of the flow (FS) measures the maximum shear within each layer in s^{-1}.

The main source of vertical shear is the bottom friction and only those layers involving the presence of the seafloor show relatively large values of FS. A good example is layer 1 (Fig. 8a) that shows only two near shore spots in CS area where FS is important, and both sites are located over the shallow seafloor. Another example is layer 6 (Fig. 8b) where FS is relatively large in ES and to the west (the only places where the flow feels the seafloor) and nearly null elsewhere.

4. Assessing of suitability of the different areas

Table 2 summarizes the findings discussed in previous section following a subjective qualification. The areas with *a priori* favorable conditions for installing marine turbine farms have been identified for each of the most suitable layers 1, 5 and 6 (column 2 in Table 2). Layer 1 shows good conditions in the eastern part of the strait and also over CS while flow properties in layers 5 and 6 are much better in the western half of the strait, particularly over CS (layer 5) and ES (layer 6). Conditions over ES in layer 5 are also favorable although to a lesser extent than in the underlying layer 6, a reason for which ES is not included in layer 5 in Table 2.

The intensity of the energy flux (I hereinafter) is the most important variable to select the right place and Table 2 indicates that all locations are rather suitable with regards to this variable, with a slightly disadvantage in the eastern strait in layer 1. CS is a good place in layers 1 and 5 due to the strength currents over the whole water column (CS is the bottleneck of the strait) but it

Table 2
Quality assessment of the variables and indicators in the favorable locations discussed in the text. The first column indicates the layer (see Table 1), the second column specifies the most suitable locations in each layer and the remaining columns refer to the different indicators, which have been rated according to: A = very good /excellent; B = good; C = medium; D = poor.

Layer	*Selected area*	*I*	*Indicators*				
			TAT	*TFP*	*TFU*	*FN*	*FS*
1	*TN*	B	C	A	A	D	B
	CS	A	B	C	C	D	B
5	*CS*	A	C	B	B	C	B
6	*ES*	A	A	A	A	B	C

Table 3
Numerical values assigned to the parameters (X_{YYY} and X_{YY}) in Eq. (3). The first block is for the restrictive indicators and the second block for the non-restrictive ones (see text). Rows X_{YYY} and X_{YY} in either block show the numerical value of the parameter which depends on the actual value of the associated indicators (I, TAT, TFP, TFU, FN and FS) discussed in the text. For instance, in a place where TAT is 65%, its associated parameter X_{TAT} would be 1, if it was 80%, X_{TAT} would be 2, and so on.

	(X_{YYY})	*Value*			
		0	*1*	*2*	*3*
Restrictive	*I* (W m^{-2})	<200	[200, 500]	[500, 800]	≥ 800
	TAT (%)	<50	[50, 75]	[75, 90]	≥ 90
	TFP (%)	<75	≥ 75	–	–
	TFU (%)	<50	[50, 80]	≥ 80	–
	(X_{YY})	*0*	*0.10*	*0.15*	*0.20*
Nonrestrictive	*FN* (m s^{-1})	<0.05	[0.05, 0.15]	[0.15, 0.25]	≥ 0.25
	FS (s^{-1})	<0.02	[0.02, 0.04]	[0.04, 0.06]	≥ 0.06

shows weaknesses regarding other indicators. Currents there are mainly bidirectional and but they show high fluctuations around the two main directions (poor rating for TFP and TFU). Moreover the periodic reversal makes TAT diminish. Additionally, CS is the place of internal wave generation, which affects the FN indicator negatively too. Except for the shear, all the defined indicators have low rating. On the contrary, ES have a very good rating for all them (except for the shear) because currents do not reverse (they maintain sign and direction) the flow tends to be supercritical there [35,55], which inhibits the upstream propagation of internal waves and, hence, propitiates a very low FN.

4.1. Quality function

In order to attempt to extract a single index of suitability from the series of the indicators computed, a quality function has been defined according to Table 2 as follows:

$$V = [2X_I^2 + X_I(X_{TAT} + X_{TFP} + X_{TFU})](1 - X_{FN})(1 - X_{FS}) \quad (3)$$

where parameters X_{YYY} quantify the different indicators according to Table 3. The numerical values of the parameters in this table aim at quantifying the qualitative rating in Table 2, assigning the value 0 to qualifier "*D*", 1 to "*C*" and so on. There are however exceptions in those parameters that appear less relevant, such as the sign of the flux, X_{TFP}, which only can take the values 0 and 1, or the directionality, X_{TFU}. On the other hand, the first three indicators defined in the previous section (TAT, TFP, and TFU) are directly related with the capability of the device to optimize the extraction of energy and their assigned indices enter Eq. (3) as summands, while the last two ones (FN and FS) are rather related to the mean life of the device and enter the equation as factors. We will call "restrictive" parameters to the first group and "non-restrictive" to the second group.

In this function, which is always positive, the energy flux weighs much more than any other parameter, since it is the main variable and appears in the equation in a single squared summand. Other parameter like TAT is of much interest and it is allowed to range from 0 to 3. The TFU, parameterized through X_{TFU}, should have more relevance for those devices that require unidirectionality of the flow, in which case the function V may be biased. Being aware of the difficulty of addressing the large variety of items to be considered in practice, we still consider that the quality function (3) summarizes the main aspects to be taken into account for decision-makers and contains enough information to help selecting the best location for energy plants based on marine currents.

The maximum values of function V found in the area are slightly greater than 30 and are located principally in the deep layer 6 over ES. Going one step ahead in the interpretation of the numerical values of V we could classify the candidate places as unfeasible ($V<15$), acceptable ($15<V<20$), advisable ($20<V<25$), and very suitable ($V>25$). Fig. 9 shows the function V in layers 1, 5 and 6, where it reaches values greater than 20 somewhere. It is readily seen that the best conditions ($V>25$ or even $V>30$) are met in layer 6 over ES, a conclusion that is easily inferred from Table 2 as well. Layer 5 shows good conditions over CS and ES, although it compares unfavorably with layer 6 in this place. CS is also the best place in layer 1 due to the strength of currents, although it is an arguable choice for devices that require unidirectionality. For this kind of devices, ES in layer 6 is the best site by far (Fig. 6b).

5. Subinertial influence

As already mentioned, meteorological forcing drives relatively important flow fluctuations at subinertial time-scale, which in turn modifies the averaged energy flux. This section estimates the effect of these fluctuations focusing on layer 6 over ES which, according to previous section, is the most suitable place from the point of view of the quality function V to install a power plant.

At subinertial time-scale, the total flow is well reproduced as the linear superposition of a mean, U_0, and meteorologically induced fluctuations, $\langle U_m(t)\rangle$ [36,46,47]. Under this assumption, $\langle U_m(t)\rangle$ averages to zero in the computation of the long-term averaged flow, and $\langle U_{total}\rangle = \langle U_0 + U_m(t)\rangle = U_0$ ($\langle\,\rangle$ indicating time average). Obviously, this result is not valid for energy flux that depends on the cube of the water velocity, which indicates that meteorologically driven fluctuations change the average energy flux.

The numerical results analyzed in this work cannot address this influence directly since the model does not include meteorological forcing. A first guess of its size can be done assuming that $U_m(t)$ is sinusoidal of frequency σ and amplitude equal to rU_0, where r is the size of the amplitude of the meteorological fluctuation relative to the mean flow, which is usually less than 1 because meteorological forcing reverses the mean flow only exceptionally [56]. Thus, $U_m(t) = rU_0 \sin(\sigma t)$ and $U_{total} = U_0(1 + r \sin(\sigma t))$. According to Eq. (1), the average energy flux would be proportional to $\langle U_{total}^3\rangle = U_0^3\langle(1 + r \sin(\sigma t))^3\rangle$. For a sinusoidal dependence, the time average between brackets, computed over a period of the fluctuation ($T = 2\pi/\sigma$) is straightforwardly computed to give $(1 + 1.5r^2)$ and, therefore $\langle U_{total}^3\rangle = (1 + 1.5r^2)U_0^3$. The first term of the parenthesis in the RHS is the energy flux in absence of meteorological forcing and the second one would be the averaged increase due to a meteorological fluctuation of relative amplitude r. A meteorological fluctuation of amplitude $r = 0.3$ that changes the

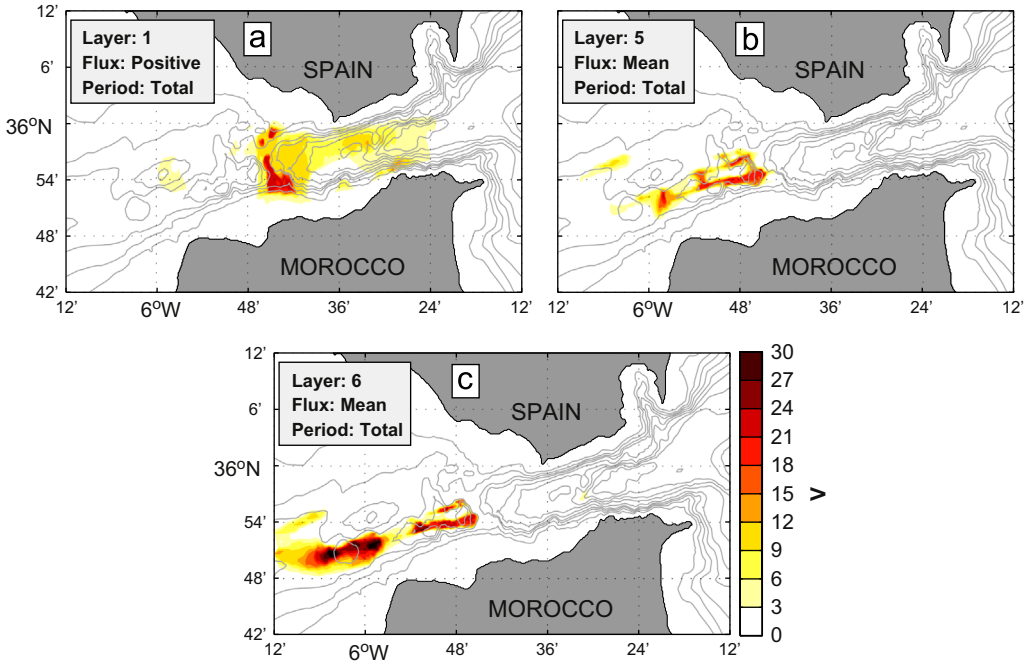

Fig. 9. Quality function (V in the text). Panels (a), (b) and (c) are for layers 1, 5 and 6, respectively.

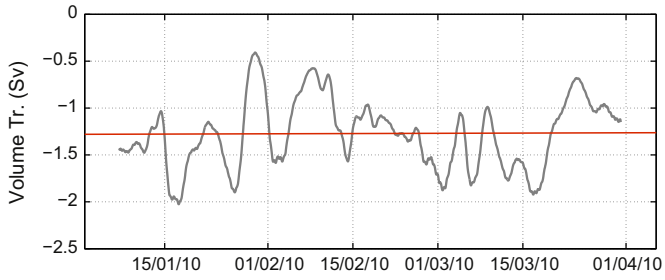

Fig. 10. Mediterranean outflow estimated from observations collected by the monitoring station of ES (see asterisk in Fig. 1). The horizontal line is the mean flow, which is around −1.3 Sv.

mean velocity up to 30% will carry out an increase of the energy flux of 0.135, that is, 13.5%.

The Mediterranean outflow has been monitored in ES since year 2004 [57], which allows us to make an approximate estimation of r directly from the observations there. Fig. 10 shows that, on average, the amplitude of the subinertial fluctuations are in the range of 0.3–0.4 Sv (Sverdrup, 1 Sv$=10^6$ m^3 s^{-1}) for a mean outflow of 1.3 Sv in absolute value, which gives a value in the range 0.25–0.31 for r. Therefore, the meteorologically forced subinertial fluctuations can increase the estimated averaged energy fluxes by a 10–15% at ES. In this location very strong currents reaching 1800 W m^{-2} have been found, hence tidal forcing contributes to overcome the intensity by 200–300 W m^{-2} but V does not change because I takes the maximum value in Table 3.

6. Summary and conclusions

The non-hydrostatic version of MIT-gcm has been implemented in a high resolution grid in the Strait of Gibraltar to estimate the energy fluxes associated with marine currents in the Strait of Gibraltar and to identify areas suitable for exploiting this renewable energy resource. The study shows that near-bottom layer over CS and ES areas and the surface layer (a subsurface shallow layer between 26 and 71 m indeed, for maritime safety reasons) over the CS and most of the eastern half of the strait gathers good conditions from the point of view of current strength. Computed averaged fluxes in these areas can exceed 1.8 kW m^{-2}.

There are other properties of the flow, however, that must be taken into account. In most areas of the strait, the tide is strong enough to reverse flows [27,29,33], a situation that may be unwanted specially for horizontal axis MCTs [9,22], but there are other areas where these reversals do not take place or, in the worst scenario, they happen very sporadically [29,38]. Also the strait is a paradigm of sheared flow and a well-known place of generation of high frequency internal waves [35], two flow properties that must be harmful for MCTs. For these reasons we have defined a set of 5 indicators that provide additional information about those flow properties that may influence the selection of a place among all places with good conditions from the point of view of the energy flux. When these indicators are considered, the surface layer shows evident weakness regarding the flow noise (an indicator defined to account for the effect of high frequency internal waves) or the directionality of the flow, since CS area is subjected to periodical flow reversals. Flow shear affects the deeper, near-bottom layers negatively due to bottom friction and tidally driven flow reversals produce undesirable fluctuations of the flow direction, which are considered harmful for the working device, etc.

For these reasons, an attempt to quantify all the influencing factors has been made by defining a quality function that prioritizes the energy flux over the rest of indicators and combines them linearly to return a single index of suitability. This function has been contoured for the layers of interest (Fig. 9) and allows us to conclude that the near-bottom layer (275–325 m depth) over ES area gathers the best conditions for installing a power plant to extract energy from marine currents. With this conclusion in mind, a short study of the meteorological influence (which was not accounted for in the model) on the estimated energy flux has been addressed by using observations collected in the very ES area. The study shows that the meteorologically-driven flow fluctuations may increase the computed energy flux in around 10–15%.

Acknowledgments

This work has been funded by the Regional Government of Junta de Andalucia (Spain) through Proyecto de Excelencia RNM-3738 (FLEGER). Partial support from CTM2010-21229-C02 of the Spanish Ministry of Economy and CTM-2008-04150E of the European MarinERA activities are also acknowledged. JCSG acknowledges a Juan de la Cierva Postdoctoral Grant (JCI-2012-13451) from the Spanish Ministry of Economy and Competitivness. We are grateful to Gianmaria Sannino from the Modelling Unit of ENEA (Italy) for his assistance in the development of the numerical model used in this study. Some of the numerical calculations presented in this work were carried out at the Supercomputing and Bioinnovation Center of the University of Málaga. This is the publication no. 51 from CEIMAR Publication Series.

References

[1] Bedard R, Jacobson PT, Previsic M, Musial W, Varley R. An overview of ocean renewable energy technologies. Oceanography 2010;23(2):22–31. http://dx.doi.org/10.5670/oceanog.2010.40.
[2] Thresher R, Musial W. Ocean renewable energy's potential role in supplying future electrical energy needs. Oceanography 2010;23(2):16–21. http://dx.doi.org/10.5670/oceanog.2010.39.
[3] Mueller M, Jeffrey H, Wallace R, von Jouanne A. Centers for marine renewable energy in Europe and North America. Oceanography 2010;23(2):42–52. http://dx.doi.org/10.5670/oceanog.2010.42.
[4] Commonwealth Scientific and Industrial Research Organisation (CSIRO). Ocean renewable energy: 2015–2050. An analysis of ocean energy in Australia. 2012.
[5] O'Rourke F, Boyle F, Reynolds A. Renewable energy resource and technologies applicable to Ireland. Renew Sustain Energy Rev 2009;13:1975–84, http://dx.doi.org/10.1016/j.rser.2009.01.014.
[6] De Falcao A. Wave energy utilization: a review of technologies. Renew Sustain Energy Rev 2010;14:899–918. http://dx.doi.org/10.1016/j.rser.2009.11.003.
[7] Drew B, Plummer AR, Sahinkaya MN. A review of wave energy converter technology. Proc Inst Mech Eng Part A: J Power Energy 2009;223:887, http://dx.doi.org/10.1243/09576509JPE782.
[8] Burman K, Walker A. Ocean energy technology overview: federal energy management program (FEMP). http://dx.doi.org/10.2172/962501.
[9] O'Rourke F, Boyle F, Reynolds A. Marine current energy devices: current status and possible future applications in Ireland. Renew Sustain Energy Rev 2010;14:1026–36. http://dx.doi.org/10.1016/j.rser.2009.11.012.
[10] O'Rourke F, Boyle F, Reynolds A. Tidal energy update 2009. Appl Energy 2010;87:398–409, http://dx.doi.org/10.1016/j.apenergy.2009.08.014.
[11] Goundar JN, Rafiuddein AM. Marine current energy resource assessment and design of a marine current turbine for Fiji. Renew Energy 2013:1–9. http://dx.doi.org/10.1016/j.renene.2013.06.036.
[12] Amelio M, Barbarelli S, Florio G, Scornaienchi NM, Minniti G, Cutrupi A, et al. Innovative tidal turbine with central deflector for the exploitation of river and sea currents in on-shore installations. Appl Energy 2012;97:944–55, http://dx.doi.org/10.1016/j.apenergy.2011.11.044.
[13] Rashid A. Status and potentials of tidal in stream energy resources in the southern coast of Iran: a case study. Renew Sustain Energy Rev 2012;16:6668–77. http://dx.doi.org/10.1016/j.rser.2012.08.010.
[14] Jo Chul hee, Yim Jin young, Lee Kang hee, Rho Yu ho. Performance of horizontal axis tidal current turbine by blade configuration. Renew Energy 2012;42:195–206, http://dx.doi.org/10.1016/j.renene.2011.08.017.
[15] Muller M, Wallace R. Enabling science and technology for marine renewable energy. Energy Policy 2008;36:4376–82. http://dx.doi.org/10.1016/j.enpol.2008.09.035.
[16] Khan MJ, Bhuyan G, Iqbal MT, Quaicoe JE. Hydrokinetic energy conversion system and assessment of horizontal and vertical axis turbines for river and tidal applications: a technology status review. Appl Energy 2009;86:1823–35, http://dx.doi.org/10.1016/j.apenergy.2009.02.017.
[17] Goude A, Agren O. Simulations of a vertical axis turbine in a channel. Renew Energy 2014;63:477–85. http://dx.doi.org/10.1016/j.renene.2013.09.038.
[18] Grogan DM, Leen SB, Kennedy CR, O'Brádaigh CM. Design of composite tidal turbine blades. Renew Energy 2013;57:151–62. http://dx.doi.org/10.1016/j.renene.2013.01.021.
[19] Liu P, Veitch B. Design and optimization for strength and integrity of tidal turbine rotor blades. Energy 2012;46:393–404. http://dx.doi.org/10.1016/j.energy.2012.08.011.
[20] Goundar JN, Rafiuddein AM. Design of a horizontal axis tidal current turbine. Appl Energy 2013;111:161–74. http://dx.doi.org/10.1016/j.apenergy.2013.04.064.
[21] Bahaj AS. Generating electricity from the oceans. Renew Sustain Energy Rev 2011;15:3399–416. http://dx.doi.org/10.1016/j.rser.2011.04.032.
[22] Li Y, Lence BJ, Calisal SM. An integrated model for estimating energy cost of a tidal current turbine farm. Energy Convers Manag 2011;52:1677–87, http://dx.doi.org/10.1016/j.enconman.2010.10.031.
[23] Funke SW, Farrel PE, Piggott MD. Tidal turbine array optimization using the adjoint approach. Renew Energy 2014;63:658–73. http://dx.doi.org/10.1016/j.renene.2013.09.031.
[24] Wang S, Yuan P, Li D, Jiao Y. An overview of ocean renewable ernergy in China. Renew Sustain Energy Rev 2011;15:91–111. http://dx.doi.org/10.1016/j.rser.2010.09.040.
[25] Ramos V, Iglesias G. Performance assessment of tidal stream turbines: a parametric approach. Energy Convers Manag 2013;69:49–57. http://dx.doi.org/10.1016/j.enconman.2013.01.008.
[26] Candela J, Winant C, Ruiz J. Tides in the Strait of Gibraltar. J Geophys Res 1990;95:7313–35.
[27] Sánchez Román A, Sannino G, García-Lafuente J, Carrillo A, Criado-Aldeanueva F. Transport estimates at the western section of the Strait of Gibraltar: a combined experimental and numerical modeling study. Geophys Res 2009;114:C06002, http://dx.doi.org/10.1029/2008JC005023.
[28] O'Rourke F, Boyle F, Reynolds A. Tidal current energy resource assessment in Ireland: current status and future update. Renew Sustain Energy Rev 2010;14:3206–12, http://dx.doi.org/10.1016/j.rser.2010.07.039.
[29] García Lafuente J, Vargas JM, Plaza F, Sarhan T, Bascheck B, Candela J. Tide at the eastern section of the Strait of Gibraltar. J Geophys Res 2000;105:14197–213.
[30] Bruno M, Alonso JJ, Cózar A, Vidal J, Ruiz Cañavete A, Echevarría F, et al. The boiling water phenomena at Camarinall Sill, the Strait of Gibraltar. Deep Sea Res II 2002;49:4097–113.
[31] Bryden Kinder. Steady two-layer exchange through the Strait of Gibraltar. Deep Sea Res 1991;38(S1):S445–63.
[32] Delgado J, García Lafuente J, Vargas JM. A simple model for submaximal exchange through the Strait of Gibraltar. Sci Mar 2001;65(4):313–22.
[33] Sannino G, Bargagli A, Artale V. Numerical modelling of the mean exchange through the Strait of Gibraltar. J Geophys Res 2002;107(C8):3094, http://dx.doi.org/10.1029/2001JC000929.
[34] Sannino G, Bargagli A, Artale V. Numerical modelling of the semidiurnal tidal exchange through the Strait of Gibraltar. J Geophys Res 2004;109:C05011, http://dx.doi.org/10.1029/2003JC002057.
[35] Sánchez Garrido JC, Sannino G, Liberti L, García Lafuente J, Pratt L. Numerical modeling of three dimensional stratified tidal flow over Camarinal Sill, Strait of Gibraltar. J Geophys Res 2011:116, http://dx.doi.org/10.1029/2011JC007093.
[36] Farmer DM, Armi L. Maximal two-layer exchange over a sill and through the combination of a sill and contraction with barotropic flow. J Fluid Mech 1986;164:53–76.
[37] García Lafuente J, Criado Aldeanueva F. Física de la Tierra. Oceanografía física: su investigación en España. Número 13. 2001.
[38] Armi L, Farmer DM. The flux of the Mediterranean water through the Strait of Gibraltar. Prog Oceanogr 1988;21:1–105.
[39] Armi L, Farmer DM. The internal hydraulics of the Strait of Gibraltar and associated sills and narrows. Oceanol. Acta 1985;8:37–46.
[40] Sánchez Garrido JC. Generación y propagación de ondas internas en el Estrecho de Gibraltar: Efectos 3-D y de rotación [PhD thesis]. University of Granada; 2009.
[41] Sánchez Garrido JC, García Lafuente J, Criado-Aldeanueva F, Baquerizo A, Sannino G. Time-spatial variability observed in velocity of propagation of the internal bore in the Strait of Gibraltar. J Geophys Res 2008:113, http://dx.doi.org/10.1029/2007JC004624.
[42] García Lafuente J, Bruque Pozas E, Sánchez Garrido JC, Sannino G, Sammartino S. The interface mixing layer and the tidal dynamics at the eastern part of the Strait of Gibraltar. J Mar Syst0924-7963 2013;117–118:31–42. http://dx.doi.org/10.1016/j.jmarsys.2013.02.014.
[43] Hanson HP, Bozek A, Duerr AE. The Florida current: a clean but challenging energy resource. EOS Trans Am Geophys Union 2011;92:29–36, http://dx.doi.org/10.1029/2011EO040001.
[44] Hanson HP, Skemp SH, Alsenas GM, Coley CE. Power from the Florida current. A new perspective on an old vision. Am Meteorol Soc 2010. http://dx.doi.org/10.1175/2010BAMS3021.1.
[45] Zhou Z, Benbouzid M, Charpentier JF, Scuiller F, Tang T. A review of energy storage technologies for marine current energy systems. Renew Sustain Energy Rev 2013;18:390–400. http://dx.doi.org/10.1016/j.rser.2012.10.006.
[46] Candela J, Winant C, Bryden HL. Meteorologically forced subinertial flows through the Strait of Gibraltar. J Geophys Res 1989;94:12667–74.
[47] García Lafuente J, Alvarez Fanjul E, Vargas JM, Ratsimandresey AW. Subinertial variability in the flow through the Strait of Gibraltar. J Geophys Res 2002;107(C10):3168, http://dx.doi.org/10.1029/2001JC001104.
[48] ⟨http://mitgcm.org/sealion/online_documents/node2.html⟩.
[49] Marshall J, Hill C, Perelman L, Adcroft A. Hydrostatic, quasi-hydrostatic and non-hydrostatic ocean modelling. J Geophys Res 1997;102:5733–52.
[50] Marshall J, Adcroft A, Hill C, Perelman L, Heisey C. A finite-volume, incompressible Navier Stokes model for studies of the ocean on parallel computers. J Geophys Res 1997:5753–66.
[51] MEDAR Group. Medatlas 2002: Mediterranean and Black Sea database of temperature, salinity and bio-chemical parameters climatological atlas. In: European Commission Marine Science and Technology Programme. Paris; 2002.
[52] Carter GS, Marriefield MA. Open boundary conditions for regional tidal simulations. Ocean Model 2007;18:194–209.
[53] Kevin AH, Fritz MH, French SP, Smith BT, Neary V. Assessment of energy production potential from tidal stream in the United States [Final project report]. Georgia Research Corporation; 2011 (DE-FG36-08G018174).

[54] ⟨http://www.tidalstreampower.gatech.edu/⟩.
[55] Sannino G, Pratt L, Carillo A. Hydraulic criticality of the exchange flow through the Strait of Gibraltar. J Phys Oceanogr 2009;39:2779–99, http://dx.doi.org/10.1175/2009JPO4075.1.
[56] Garcia Lafuente J, Delgado J, Criado F. Inflow interruption by meteorological forcing in the Strait of Gibraltar. Geophys Res Lett 2002;29:19.
[57] Naranjo C, García Lafuente J, Sánchez Garrido JC, Sánchez Román A, Delgado Cabello J. The Western Alboran Gyre helps ventilate the Western Mediterranean Deep Water through Gibraltar. Deep Sea Res Part I: Ocean Res Pap 2012;63:157–63. http://dx.doi.org/10.1016/j.dsr.2011.10.003.